Hindawi
Advances in Materials Science and Engineering
Volume 2019, Article ID 9359410, 12 pages
https://doi.org/10.1155/2019/9359410

Research Article

Crack Initiation Criteria and Fracture Simulation for Precracked Sandstones

R. Q. Huang, L. Z. Wu, and B. Li

State Key Laboratory of Geohazard Prevention and Geoenvironment Protection, Chengdu University of Technology, Chengdu, Sichuan 610059, China

Correspondence should be addressed to L. Z. Wu; wulizhou07@mail.cdut.edu.cn

Received 25 November 2018; Revised 6 May 2019; Accepted 4 June 2019; Published 4 August 2019

Academic Editor: Raffaele Sepe

The friction coefficient, tip curvature, and different-width crack state influence the stress intensity factor (SIF). The maximum circumferential tensile stress (MTS) and minimum strain energy density criterion (S) face challenges in explaining the mode-II fracture propagation of cracks. The maximum radial shear stress (MSS) and modified twin shear stress factor (ITS) criteria are proposed as the brittle mode-II fracture criteria. The experiments and numerical analysis are also performed. The results indicate that the fracture angles of the MSS and ITS were similar and different from the results of MTS and S. The equivalent stress intensity factors (ESIFs) from the mixed mode I-II are proposed to determine the fracture mode. There are different fracture models for different cracks under tensile and compressive stresses. The ratio of the tensile strength to uniaxial compressive strength influenced the fracture angle of ITS. The lateral pressure coefficient (k) had a significant effect on the mode-II fracture angle when the angle between the crack and the vertical direction is less than 40° and the lateral pressure coefficient is more than 0. Because the same fracture mode k ($k > 0$) can inhibit mode-I fracturing, conversely, it can also promote mode-I fracturing. Experimental results and numerical simulations of fracture propagation under uniaxial compression confirmed that the theoretical results were correct.

1. Introduction

Rock develops in complex geological environments and includes various defects or flaws. These flaws weaken the mechanical properties of the rock mass and modify the stress distributions. Internal cracks in rock mass exert an important effect on determining the fracture mode, initiation, propagation, and rock strength [1–9].

The cracks in a rock mass can be divided into three basic modes: mode-I crack (normal load), mode-II crack (shear load), and mode-III crack (antiplane shear load). A tensile, shear, and tear crack fracture is defined as a mode I, II, and III fracture, respectively [10]. The mixed mode I-II is the most common type of a mixed mode fracture. After fracture mechanics was introduced into rock mechanics, the SIF was employed to describe the stress state at the crack tip [11]. When the shear stress acting on the main crack exceeds the friction stress between the cracks, the stress will concentrate at the crack tip. The cracks continue to grow and curve toward the direction of the maximum principal stress, when the stress strength factor meets or exceeds K_{IC}. Based on the maximum shear stress theory, a method has been proposed to compute the crack initiation angle under a mixed mode I-II fracture [12]. The open-type crack geometry influences crack propagation [12, 13]. The crack initiation and growth on a rock specimen subjected to compressive stress has been investigated experimentally [1, 3, 7, 14–26]. Many numerical methods have been used to analyze the fracture and crack propagation in rocks, such as the finite element method (FEM), boundary element method (BEM), and discrete element method (DEM). By using the finite element fracture software called Franc2D, the energy release rate (G), crack propagation, fracturing time, and static tensile and normal-distributed stresses were calculated to represent the crack initiation and growth in a rock specimen [11, 27]. A realistic failure process analysis has been developed to simulate the cracked rock failure [28]. The PFC2D software has been employed to discuss the effect of the initial flaw orientation

in the specimen's failure mode under compressive loading [29]. A fracture and crack propagation analysis system has been employed in the investigation of crack growth [30]. The maximum tangential stress [31], maximum energy release rate [32], and minimum energy density criterion [33, 34] have typically been considered as the fracture initiation criteria to identify the crack growth mechanism of brittle rocks. The F-criterion and modified energy release rate criterion have also been used to investigate quasi-brittle fracture characteristics [35–37].

These criteria are based on the assumption of a mode-I fracture. However, the mode-II fracture extension of compression-shear cracks has rarely been investigated. Approaches toward identifying a fracture mode that can determine suitable fracture criteria are lacking. Therefore, it is difficult to determine the fracture mode of a crack and the modes I, II, or III fracture toughness according to experimental results.

The main objective of this paper was to propose a mode-II fracture criterion and conduct a numerical analysis of an open and closed brittle rock cracks. Mixed mode I-II ESIFs are proposed to determine the fracture mode. The relationships between the fracture angle and model of crack propagation with a crack angle and thickness, lateral pressure coefficient, and ratio of tensile strength to compressive strength are discussed. The consistency between the theoretical and numerical results was verified.

2. SIF of Mixed Mode I-II Crack

According to the linear elastic method, the stress components of the mixed mode I-II at the crack tip in the polar coordinates can be expressed as follows [38]:

$$\sigma_r = \frac{1}{2\sqrt{2\pi r}}\left[K_{\mathrm{I}}\cos\frac{\theta}{2}(3-\cos\theta)+K_{\mathrm{II}}\sin\frac{\theta}{2}(3\cos\theta-1)\right], \tag{1a}$$

$$\sigma_\theta = \frac{1}{2\sqrt{2\pi r}}\cos\frac{\theta}{2}\left[K_{\mathrm{I}}(1+\cos\theta)-3K_{\mathrm{II}}\sin\theta\right], \tag{1b}$$

$$\tau_{r\theta} = \frac{1}{2\sqrt{2\pi r}}\cos\frac{\theta}{2}\left[K_{\mathrm{I}}\sin\theta+K_{\mathrm{II}}(3\cos\theta-1)\right], \tag{1c}$$

where K_{I} is the mode-I SIF, K_{II} is the mode-II SIF, r is the distance from the crack tip, and θ is the angle by which the surface deviates from the original crack tip direction.

An infinite plate with a central crack under biaxial loading (σ_y^∞ and σ_x^∞, $\sigma_x^\infty = k\sigma_y^\infty$) is shown in Figure 1, where the crack length is $2a$. The stress state along the crack plane can be determined as follows:

$$\sigma_{\mathrm{T}} = \sigma_y^\infty\cos^2\beta+\sigma_x^\infty\sin^2\beta, \tag{2a}$$

$$\sigma_{\mathrm{N}} = \sigma_y^\infty\sin^2\beta+\sigma_x^\infty\cos^2\beta, \tag{2b}$$

$$\tau = \left(\sigma_y^\infty-\sigma_x^\infty\right)\sin\beta\,\cos\beta, \tag{2c}$$

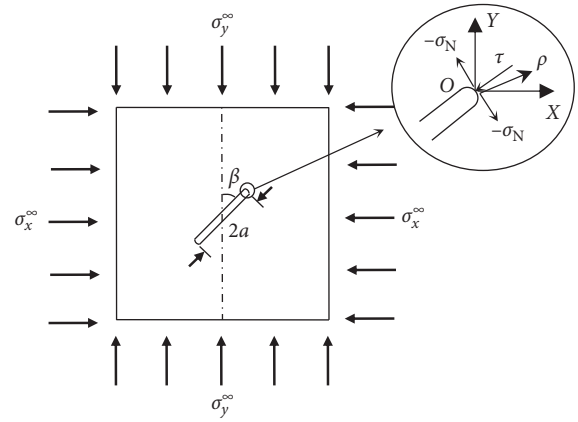

Figure 1: External and internal stresses for mixed mode I-II crack in infinite plate.

where σ_{T}, σ_{N}, and τ are the tangential stress, normal stress, and shear stress. The tensile stress is positive, while the compressive stress is negative.

The SIF for cracks with different widths, which causes friction and no friction along the crack plane, is different. K_{IT} and K_{IN} are SIF generated by the transverse compressive stress and normal stress, respectively. K_{IT} is only considered when the transverse compressive stress $\sigma_{\mathrm{T}} < 0$, and $K_{\mathrm{IT}} = -(1/2)\sigma_{\mathrm{T}}\sqrt{\rho/a}\sqrt{\pi a}$ when $\rho/a \longrightarrow 0$. In addition, $K_{\mathrm{IN}} = \sigma_{\mathrm{N}}\sqrt{\pi a}$. Mode-I SIF ($K_{\mathrm{I}}$) is only considered when the crack is tensile ($\sigma_{\mathrm{N}} > 0$) for a closed crack (causing friction), and $K_{\mathrm{I}} = 0$ when $\sigma_{\mathrm{N}} \le 0$. Mode-I SIF is affected by the crack tip radius of curvature (ρ) and the transverse compressive stress (σ_{T}) for a nonclosed crack (no friction along the crack plane) [39] (Figure 1), but $K_{\mathrm{I}} \le 0$ for $\sigma_{\mathrm{N}} \le 0$. K_{I} exerts an inhibitory effect on the circumferential stress of mode-II SIF (K_{II}). Table 1 lists the results of calculating SIF for closed and nonclosed cracks.

3. Fracture Criterion of Brittle Material

3.1. Maximum Circumferential Tensile Stress Theory (MTS). The maximum circumferential tensile stress criterion can effectively explain the tensile fracture of brittle rock. The crack propagation direction at the crack tip can be obtained by using the maximum circumferential stress [31]. The equivalent mode-I stress intensity factor (K_{Ie}), which is transformed from the mixed mode I-II fracture, is defined as follows:

$$K_{\mathrm{Ie}} = \frac{1}{2}\cos\frac{\theta_0}{2}\left[K_{\mathrm{I}}(1+\cos\theta_0)-3K_{\mathrm{II}}\sin\theta_0\right], \tag{3}$$

where the initiation angle $\theta_0 = 2\arctan\left((1-\sqrt{1+8(K_{\mathrm{I}}/K_{\mathrm{II}})^2})/(4K_{\mathrm{II}}/K_{\mathrm{I}})\right)$.

When K_{Ie} equals the mode-I fracture toughness (K_{IC}), the crack initiates, and K_{I} is 0 for a closed crack. Thus, $\theta_0 = 70.5^\circ$ (when $K_{\mathrm{II}}/K_{\mathrm{I}} \longrightarrow \infty$, $\lim_{K_{\mathrm{II}}/K_{\mathrm{II}}\longrightarrow\infty}(1-\sqrt{1+8(K_{\mathrm{II}}/K_{\mathrm{I}})^2})/(4K_{\mathrm{II}}/K_{\mathrm{I}}) = 1/\sqrt{2}$, thus $\theta_0 = 70.5^\circ$), and K_{Ie} becomes maximum for closed cracks.

Table 1: SIFs for closed and nonclosed cracks.

Crack thickness (mm)	Loading conditions	K_{IN}	K_{IT}	K_I	K_{II}
0.5	$\sigma_N > 0$	$\sigma_N\sqrt{\pi a}$	0	$K_{IN} + K_{IT}$	$\tau\sqrt{\pi a}$
	$\sigma_N < 0,\ \lvert\tau\rvert > u\lvert\sigma_N\rvert$	0	0	$K_{IN} + K_{IT}$	$(\lvert\tau\rvert - u\lvert\sigma_N\rvert)\sqrt{\pi a}$
	$\sigma_N < 0,\ \lvert\tau\rvert \le u\lvert\sigma_N\rvert$	0	0	$K_{IN} + K_{IT}$	0
2.0	$\sigma_T < 0$	$\sigma_N\sqrt{\pi a}$	$-(1/2)\sigma_T\sqrt{\rho/a}\sqrt{\pi a}$ $(\rho/a \longrightarrow 0)$,	$K_{IN} + K_{IT}$	$\tau\sqrt{\pi a}$
	$\sigma_T > 0$	$\sigma_N\sqrt{\pi a}$	0	$K_{IN} + K_{IT}$	$\tau\sqrt{\pi a}$

3.2. Minimum Strain Energy Density Criterion (S). The fracture angle of the crack is determined by the direction of the minimum strain energy density, and the strain energy density of a near crack tip element is expressed as follows [40]:

$$S = a_{11}K_I^2 + 2a_{12}K_IK_{II} + a_{22}K_{II}^2 + a_{33}K_{III}^2, \tag{4}$$

where K_{III} is the mode-III SIF ($K_{III} = 0$) and a_{11}, a_{12}, a_{22}, and a_{33} can be obtained as follows:

$$a_{11} = \frac{1}{16\pi\mu}(3 - 4\nu - \cos\theta)(1 + \cos\theta), \tag{5a}$$

$$a_{12} = \frac{1}{8\pi\mu}(\cos\theta - 1 + 2\nu)\sin\theta, \tag{5b}$$

$$a_{22} = \frac{1}{16\pi\mu}[4(1-\nu)(1-\cos\theta) + (1+\cos\theta)(3\cos\theta - 1)], \tag{5c}$$

$$a_{33} = \frac{1}{4\pi\mu}, \tag{5d}$$

where μ is the shear modulus and ν is Poisson's ratio. The initiation angle (θ_0) can be obtained by $\partial S/\partial\theta = 0$ and $\partial^2 S/\partial\theta^2 > 0$.

There exist more fracture criteria, including the maximum potential energy release rate criterion and energy-momentum tensor criterion. However, these fracture criteria require a mode-I fracture. Therefore, the radial shear stress criterion and modified twin shear stress factor criterion for a mode-II fracture are proposed.

3.3. Maximum Radial Shear Stress Criterion (MSS). The maximum radial shear stress at the crack tip should satisfy the following [41]:

$$\frac{\partial\tau_{r\theta}}{\partial\theta} = 0, \quad \frac{\partial^2\tau_{r\theta}}{\partial\theta^2} < 0 \text{ or } \frac{\partial^2\tau_{r\theta}}{\partial\theta^2} > 0,\ \left|\tau_{r\theta}(\theta = \theta_0)\right|_{\max}. \tag{6}$$

θ_0 is expressed as follows:

$$\theta_0 = 2\arctan\left(\frac{-2 + \sqrt{A}\left(\cos(\alpha_0/3) - \sqrt{3}\sin(\alpha_0/3)\right)}{3k_0}\right), \tag{7}$$

where $A = 4 + 42(K_{II}/K_I)^2$, $B = -4(K_{II}/K_I)$, $\alpha_0 = \arccos(T)$, $T = (-4A - 3k_0B)/2\sqrt{A^3}$, $k_0 = 2(K_{II}/K_I)$, and $(\alpha_0 \in (0, \pi)$, $-1 < T < 1)$.

3.4. Modified Twin Shear Stress Factor Criterion (ITS). The twin shear stress factor criterion can be used to analyze the initiation angle of a pure mode-I fracture. However, there is significant deviation in the investigation of a mixed mode I-II fracture. Moreover, an improved twin shear stress factor criterion is proposed to predict the mode-II fracture angle.

For 2D plane strain problems, the principal stresses σ_1 and σ_3 can be determined as follows:

$$\sigma_{1,3} = \left(\frac{1}{2}(\sigma_r + \sigma_\theta)\right) \pm \left(\frac{1}{2}\sqrt{(\sigma_r - \sigma_\theta)^2 + 4\tau_{r\theta}^2}\right). \tag{8}$$

Based on equation (8), σ_2 can be obtained by assuming plane strain ($\varepsilon_2 = 0$). This can satisfy $\sigma_1 > \sigma_2 > \sigma_3$.

The twin shear stress f can be determined by the shear stresses τ_{12}, τ_{13}, and τ_{23}, as follows:

$$f = \tau_{13} + \alpha\tau_{12} = \frac{\sigma_1}{2}(1 + \alpha) - \frac{1}{2}(\alpha\sigma_2 + \sigma_3), \quad \tau_{12} > \tau_{23}, \tag{9a}$$

$$f = \tau_{13} + \alpha\tau_{12} = \frac{1}{2}(\sigma_1 + \alpha\sigma_2) - \frac{\sigma_3}{2}(\alpha + 1), \quad \tau_{12} < \tau_{23}, \tag{9b}$$

where the principle shear stresses can be expressed as $\tau_{12} = 0.5(\sigma_1 - \sigma_2)$, $\tau_{23} = 0.5(\sigma_2 - \sigma_3)$, and $\tau_{13} = 0.5(\sigma_1 - \sigma_3)$ and α is the ratio of σ_t to σ_c of the rocks such that $\alpha = \sigma_t/\sigma_c$.

By substituting equations (1a)–(1c) and (8) into equations (9a) and (9b), f can be expressed as follows:

$$f = \frac{1}{2\sqrt{2\pi r}}T_s(K_I, K_{II}, \theta), \tag{10}$$

where $T_s(K_I, K_{II}, \theta)$ is the twin shear stress factor.

The shear stress is constant ($C = \tau_{r\theta}$) on the radial shear stress line, and f on the equal radial shear stress line stress can be expressed as follows:

$$f = CF(K_I, K_{II}, \theta), \tag{11}$$

where $F(K_I, K_{II}, \theta)$ is given by

$$F(K_I, K_{II}, \theta) = \frac{T_s(K_I, K_{II}, \theta)}{\cos\theta/2\left[K_I\sin\theta + K_{II}(3\cos\theta - 1)\right]}. \tag{12}$$

The crack fractures along the direction of the twin shear stress minimum value, and the fracture angle are given by

$$\frac{\partial F}{\partial \theta} = 0, \quad \frac{\partial^2 F}{\partial \theta^2} < 0, \quad F < 0,\ C < 0. \tag{13}$$

The equivalent mode-II SIF that transforms from the mixed mode I-II fracture can be expressed as follows:

$$K_{\mathrm{IIe}} = \frac{1}{2}\cos\frac{\theta_0}{2}\left[K_{\mathrm{I}}\sin\theta_0 + K_{\mathrm{II}}\left(3\cos\theta_0 - 1\right)\right]. \tag{14}$$

4. Fracture Mode and Fracture Criterion

4.1. Identification of Fracture Mode. The dimensionless stress field at the crack tip can be expressed as follows [42]:

$$f_\theta = \frac{\sigma_\theta\sqrt{2r}}{\sqrt{a\left(\sigma_y^\infty + \sigma_x^\infty\right)^2}}, \tag{15a}$$

$$f_{r\theta} = \frac{\tau_{r\theta}\sqrt{2r}}{\sqrt{a\left(\sigma_y^\infty + \sigma_x^\infty\right)^2}}. \tag{15b}$$

For most rocks, K_{IC} is less than K_{IIC} [43]. The fracture mode can be determined according to the relationship between the stress field and fracture toughness.

The dimensionless stress field of the mixed mode I-II crack is shown in Figure 2. We can obtain $f_{\theta\max} > |f_{r\theta\max}|$ for the modes I ($\sigma_{\mathrm{N}} > 0$) and II crack shown in Figures 2(a) and 2(c), i.e., $K_{\mathrm{Ie}}/|K_{\mathrm{IIe}}| > K_{\mathrm{IC}}/K_{\mathrm{IIC}}$. Thus, a mode-I fracture occurs. However, there exists $f_{\theta\max} < |f_{r\theta\max}|$ for the mode-I crack without friction along the crack plane ($\sigma_{\mathrm{N}} < 0$), that is, $K_{\mathrm{Ie}}/|K_{\mathrm{IIe}}| < 0 < K_{\mathrm{IC}}/K_{\mathrm{IIC}}$, which occurs with the mode-II fracture.

For a mixed mode I-II crack, K_{I} and K_{II} are superimposed. The circumferential stress field occurs according to Figures 2(a) and 2(c). If $\sigma_{\mathrm{N}} > 0$, $K_{\mathrm{Ie}}/|K_{\mathrm{IIe}}| > K_{\mathrm{IC}}/K_{\mathrm{IIC}}$, a mode-I fracture occurs. Otherwise, the circumferential stress decreases according to Figures 2(b) and 2(c), when $\sigma_{\mathrm{N}} < 0$. The circumferential stress field is the same as that shown in Figure 2(c) for a mixed mode I-II closed crack, when $\sigma_{\mathrm{N}} < 0$. Thus, $K_{\mathrm{Ie}}/|K_{\mathrm{IIe}}| > K_{\mathrm{IC}}/K_{\mathrm{IIC}}$ and the fracture is mode-I. For a mixed mode I-II crack without friction, when $\sigma_{\mathrm{N}} < 0$, the fracture mode can be expressed as follows:

$$K_{\mathrm{Ie}} < 0, \quad \text{for mode} - \text{II} - \text{fracture}, \tag{16a}$$

$$\frac{K_{Ie}}{|K_{\mathrm{IIe}}|} > 1, \quad \text{for mode} - \text{I} - \text{fracture}, \tag{16b}$$

$$\frac{0 < K_{Ie}}{K_{\mathrm{IIe}} < 1}, \ \frac{K_{Ie}}{K_{\mathrm{IIe}}} > \frac{K_{IC}}{K_{\mathrm{IIC}}}, \quad \text{for mode} - \text{I fracture}, \tag{16c}$$

$$\frac{0 < K_{Ie}}{K_{\mathrm{IIe}} < 1}, \ \frac{K_{Ie}}{K_{\mathrm{IIe}}} < \frac{K_{IC}}{K_{\mathrm{IIC}}}, \quad \text{for mode} - \text{II fracture}. \tag{16d}$$

4.2. Example: Mixed Mode I-II Nonclosed Crack under Compression. By assuming that the crack aperture was 2 mm, the crack length was $2a = 10$ mm, the curvature radius was $\rho = 1$ mm at the crack tip, and the crack was nonclosed during loading. The relationship between the crack angles and the fracture angles is shown in Figure 3, where the mixed mode I-II nonclosed crack was analyzed according to MTS, *S*, MSS, and ITS. The fracture angles based on MTS and *S* were similar. The fracture angles based on *S* were influenced by ν; however, the results were quite different when $\beta < 40^\circ$ and $k < 0$. Otherwise, the fracture angles between MSS and ITS were similar and the fracture angles from ITS were influenced by $\alpha = \sigma_{\mathrm{t}}/\sigma_{\mathrm{c}}$. The lateral pressure coefficient ($k > 0$) exerted a significant effect on the mode-II fracture angle when $\beta < 40^\circ$ (Figures 3(a) and 3(b)).

The mode I-II fracture regions for the mixed mode I-II nonclosed cracks (equations (16a)–(16d)) are shown in Figure 4. k exerted a significant effect on the fracture mode. The positive k ($k > 0$) value inhibited the mode-I fracture (Figures 4(a) and 4(b)), while the negative k value promoted the mode-I fracture (Figures 4(a) and 4(c)).

The criteria selected to analyze the fracture angles of the crack were based on the fracture mode. In the mode-I fracture, the fracture criteria, such as MTS and *S*, could forecast the fracturing angle. Moreover, the MSS and ITS criteria are suggested for the mode-II fracture.

5. Numerical Analysis and Experimental Results of Single-Crack Sample Failure

5.1. Numerical Model. The SIF of a single-crack sandstone was investigated by using a finite element software ABAQUS. Using the commercial finite element software, the extended FEM and a cohesive model were employed to simulate the crack propagation for a single-crack rock without considering the progressive process [44, 45]. The Benzeggagh–Kenane (B-K) model can be expressed as follows [46]:

$$G_{\mathrm{TC}} = G_{\mathrm{IC}} + \left(G_{\mathrm{IIC}} - G_{\mathrm{IC}}\right)\left(\frac{G_{\mathrm{s}}}{G_{\mathrm{T}}}\right)^{\eta}, \tag{17}$$

where η is the material parameter and G_{IC} and G_{IIC} are the energy release rates of the mode I-II fracture, $G_{\mathrm{s}} = G_{\mathrm{II}} + G_{\mathrm{III}}$, $G_{\mathrm{T}} = G_{\mathrm{I}} + G_{\mathrm{s}}$, and $G_{\mathrm{TC}} = 0.5\sigma_0 u_{\mathrm{f}}$, σ_0 is the stress threshold of the crack fracture, and u_{f} is the displacement of the cohesive model when fracture occurs.

The computational models of the rock samples are described in Figure 5. The mechanical simulation analysis parameters are listed in Table 2. The SIF of a single crack was obtained numerically based on the elasticity theory, by applying a compressive stress of 10 MPa and $k = 0$. A collapse element was employed to simulate the singularity of the crack tip.

Table 3 depicts the changes in the maximum circumferential stress and the radial shear stress at the crack tip. Figures 6–8 show the computational results of a single-crack brittle rock fracture with different precracked angles.

5.2. Analysis of Closed Crack Fracture. When the crack angle was smaller, the crack extended with a small angle (1–5 in

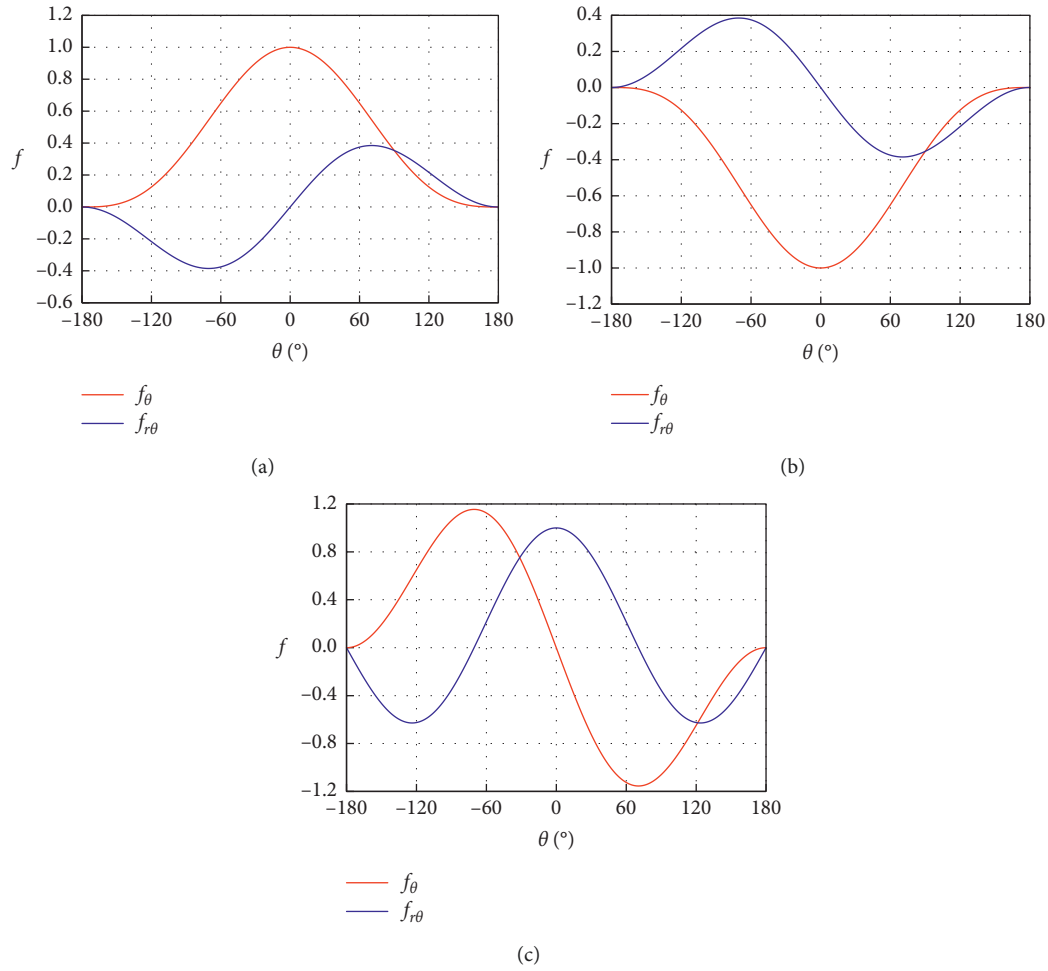

Figure 2: Dimensionless stress field of mode I-II crack: (a) mode-I crack with friction, $\sigma_N > 0$; (b) mode-I crack without friction,$\sigma_N < 0$; (c) mode-II crack.

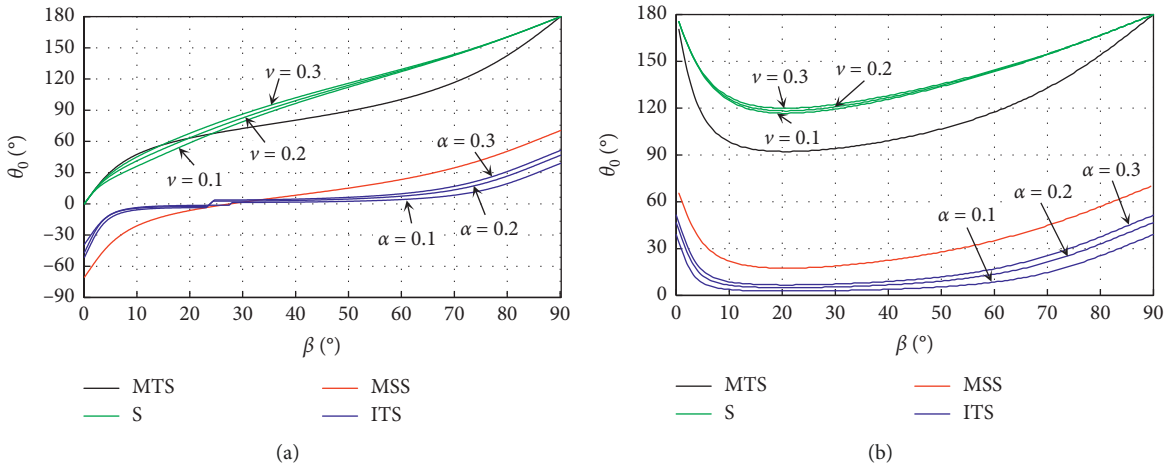

Figure 3: Continued.

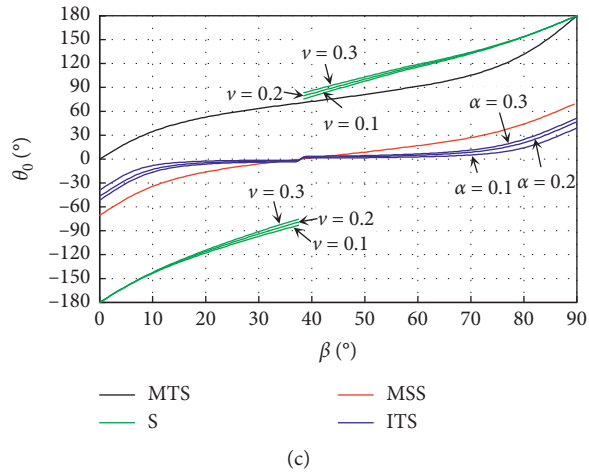

(c)

Figure 3: Relationship between crack angle and fracture angle for mixed mode I-II nonclosed crack: (a) $\sigma_y^\infty < 0$, $k = 0$; (b) $\sigma_y^\infty < 0$, $k = 0.4$; (c) $\sigma_y^\infty < 0$, $k = -0.4$.

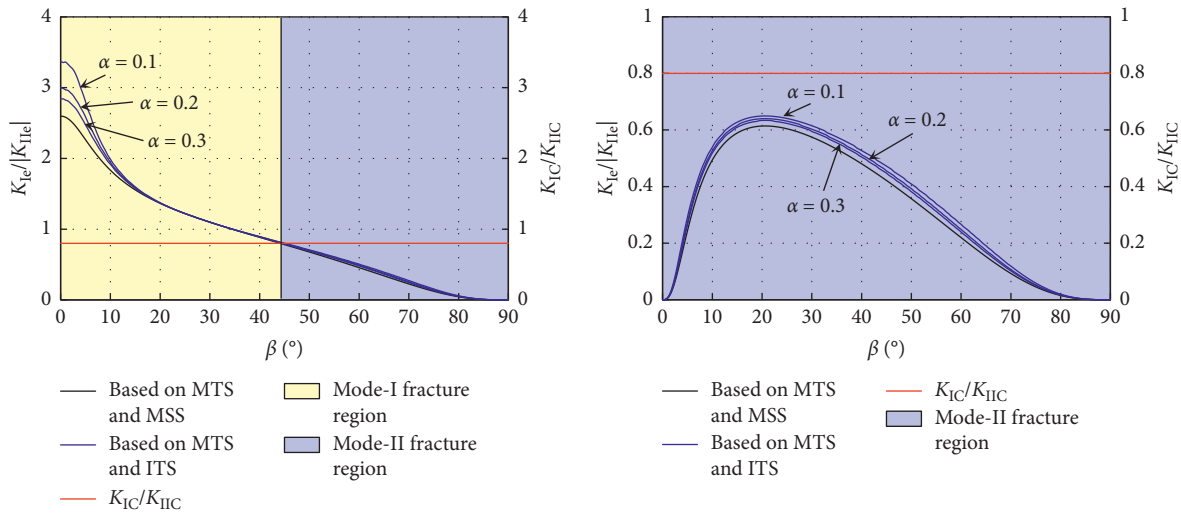

(a) (b)

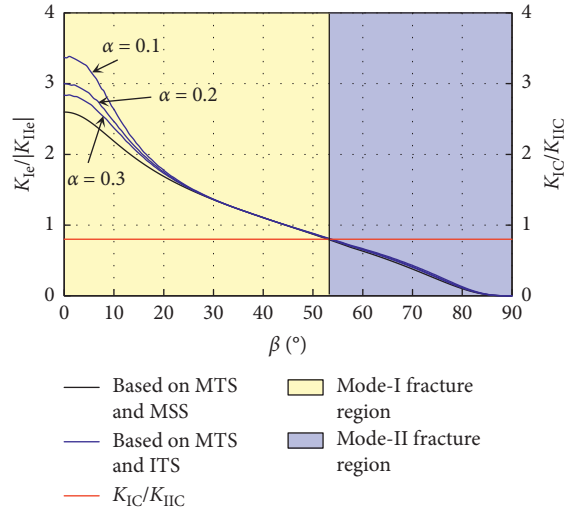

(c)

Figure 4: Mode I-II fracture regions for mixed mode I-II nonclosed cracks: (a) $\sigma_y^\infty < 0$, $k = 0$; (b) $\sigma_y^\infty < 0$, $k = 0.4$; (c) $\sigma_y^\infty < 0$, $k = -0.4$.

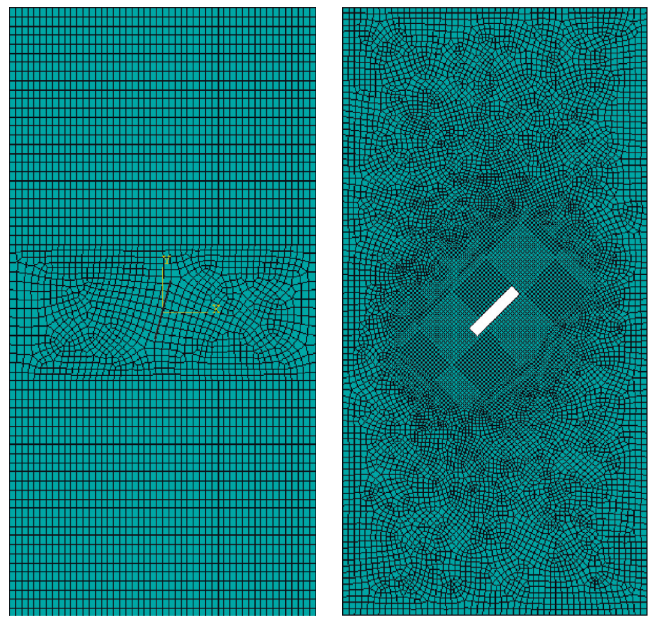

(a) (b)

Figure 5: Calculation model diagram of single-crack sample ($r = 0$): (a) closed crack: crack angle $\beta = 15^{\circ}$, crack thickness $d = 0.5$ mm; (b) nonclosed crack: crack angle $\beta = 45^{\circ}$, crack thickness $d = 2$ mm.

Table 2: Numerical parameters for analysis.

Material	Elastic modulus E (GPa)	Friction coefficient u	Poisson's ratio ν	G_{IC} (N/mm)	G_{IIC} (N/mm)	η	Maximum nominal stress of type I failure N_{max} (MPa)	Maximum nominal stress of type II failure S_{max} (MPa)	Maximum nominal stress of type III failure T_{max} (MPa)
Brittle material	1.354	0.12	0.21	0.62	0.76	1.0	6.63	8.09	8.09

Table 3), rather than with an angle of 70.5°, from the maximum circumferential stress theory. This was caused by the strong influence of material expansion, which was in turn caused by compression. Therefore, equation (1b) cannot be used to calculate the circumferential stress with a small crack angle. However, the material expansion had a smaller effect on the stress field at the crack tip, when the crack angle was greater than 15°. By using the maximum circumferential stress criterion, the fracture initiation angles in the experiments were approximately 70.5°. Therefore, equation (1b) could be used to calculate the circumferential stress in a rock with crack angles greater than 15°.

The results revealed that the material expansion exerted a considerable effect on the stress at the crack tips, when the crack angle was small and the initiation angles gradually approached 70.5°, according to the maximum circumferential stress theory. Therefore, the maximum circumferential stress theory can be used to estimate the fracture criterion and calculate the compression-induced initiation angles for the closed cracks, if the crack angle is greater than 15°.

5.3. Fracture Analysis of Nonclosed Crack. The mode-I SIF of the nonclosed crack was negative when the crack was under compression ($\sigma_N < 0$). According to equation (1), the mode-I circumferential compressive stress with $K_I < 0$ at the crack tip will restrain the circumferential tensile stress caused by the mode-II SIF. The maximum circumferential tensile stress at the crack tip was less than the radial shearing stress under certain conditions. Thus, the mode-II fracture in a nonclosed crack occurred only if $0 < K_{Ie}/|K_{IIe}| < 1$ and $K_{Ie}/|K_{IIe}| < K_{IC}/K_{IIC}$. Therefore, the mode domain could be divided into two regions, namely, the mode-I and mode-II fracture regions (Figure 4). Figure 9 represents the crack propagation between numerical and experimental results where crack thickness is 2 mm. The tests were carried out on an MTS815 test system (MTS Systems Corporation, Eden Prairie, MN, USA). The sample was from rock-like material with 2 mm thick crack with a width of 50 mm. The testing and numerical results show that the initiation angle of the crack and fracture propagation are similar. Figure 10 compares the initiation angles between the theoretical analysis and numerical results when $\sigma_y^{\infty} < 0$ and $k = 0$. The testing results indicate that fracture criteria for predicting the crack propagation is closely related to precracked angle.

The mode-I fracture occurred in a sample with a nonclosed crack, when the crack angle was less than 45° (Figure 4(a)). The crack rupture angles were small, which does not agree with the initiation angles (70.5°) obtained by the MTS and listed in Table 3. For crack angles greater than 30°, there existed considerable differences between the fracture angles of the closed and nonclosed cracks (Figure 8),

Table 3: Numerical results of stress near the crack tip.

Condition	Crack thickness d (mm)	Crack angle β (°)	Maximum circumferential stress at crack tip (MPa)	Direction of the maximum circumferential stress (°)	Maximum radial shear stress at crack tip (MPa)	Direction of the maximum radial shear stress (°)
1		15	10.258	13	8.206	0
2		30	13.057	47	10.435	0
3	0.5	45	14.984	63	11.981	0
4		60	12.731	65	10.193	0
5		75	11.726	73	9.437	0
6		15	13.127	34	8.533	−10
7		30	15.424	45	14.677	2
8	2.0	45	12.387	81	17.749	7
9		60	7.742	101	17.066	12
10		75	1.548	125	14.678	41

The tip radius of curvature is 0.25 mm for conditions 1–5 and 1.0 mm for conditions 6–10.

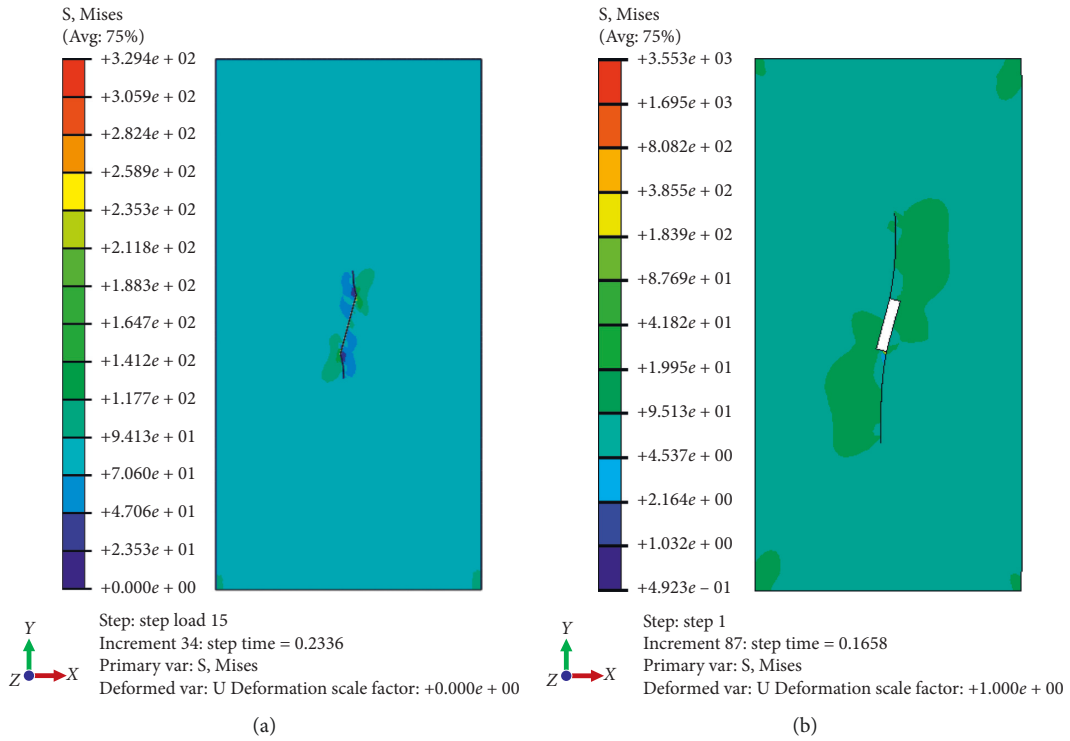

Figure 6: Numerical simulation of fracture propagation with $\beta = 15°$: (a) 0.5 mm thick crack ($\rho = 0.25$ mm); (b) 2.0 mm thick crack ($\rho = 1.0$ mm).

and the rupture angles of the open cracks were similar to the results obtained by the MSS and ITS (Figure 10). Therefore, the identification of the fracture mode and proposed mode-II fracture criteria is correct.

The analysis revealed that the maximum circumferential stress criterion faces challenges in describing the fracture growth of open cracks subject to compression. The initiation angles could be determined by the radial shear stress criterion if $0 < K_{Ie}/|K_{IIe}| < 1$ and $K_{Ie}/K_{IIe} < K_{IC}/K_{IIC}$ were satisfied.

6. Conclusions

The mode-II fracture criteria and a method of fracture mode identification were proposed. We conducted a uniaxial compression numerical analysis on brittle material containing closed and open cracks at various angles and thicknesses. The numerical and theoretical results were analyzed and the following conclusions were drawn:

(1) The fracture angles, based on the MSS and ITS, were close. The ITS results were influenced by the ratio of the tensile strength to the uniaxial compressive strength of the rocks. k exerted an important effect on the mode-II fracture angle. A positive k value inhibited the mode-I fracture, while a negative k value promoted the mode-I fracture.

(2) Friction caused by crack thickness has an important role in the fracture initiation angle. The initiation direction of the closed crack at the crack tip

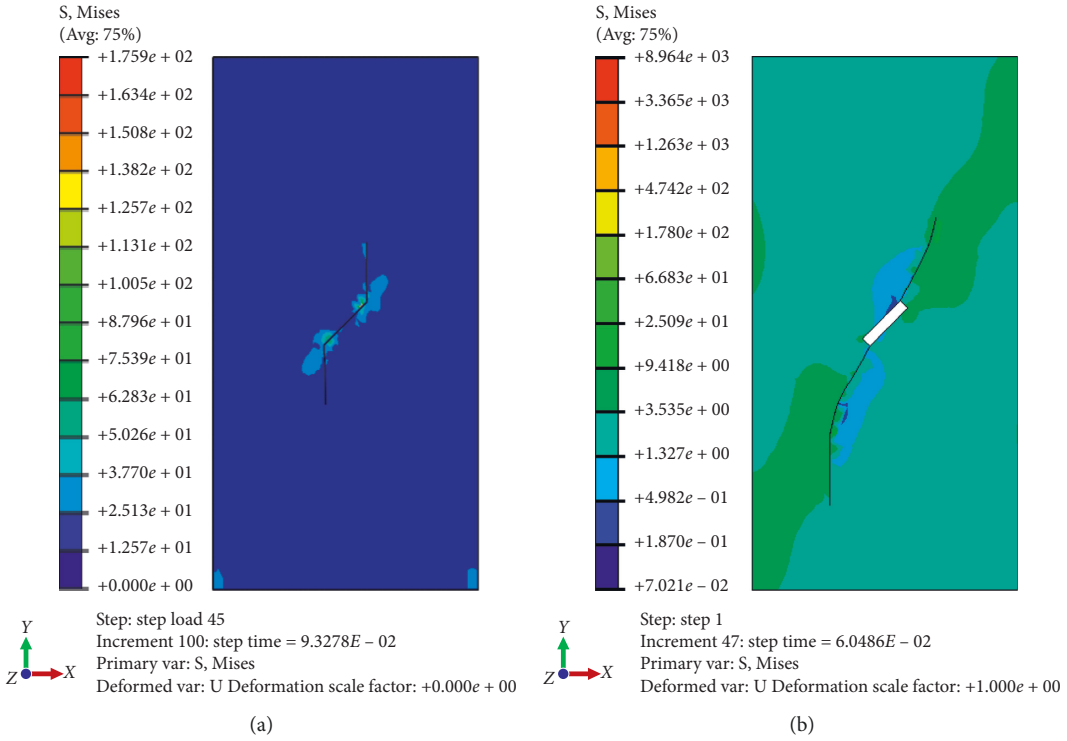

FIGURE 7: Numerical simulation results of single-crack fracture propagation with $\beta = 45°$: (a) 0.5 mm thick crack ($\rho = 0.25$ mm); (b) 2.0 mm thick crack ($\rho = 1.0$ mm).

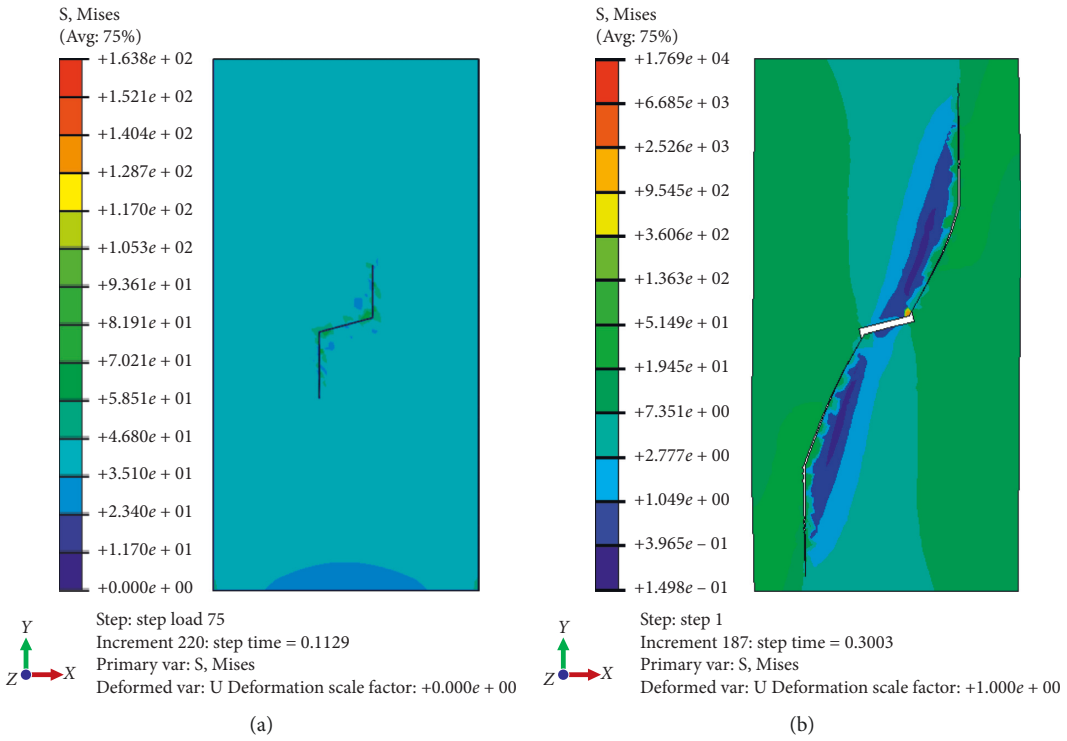

FIGURE 8: Numerical simulation results of single-crack fracture propagation with $\beta = 75°$: (a) 0.5 mm thick crack ($\rho = 0.25$ mm); (b) 2.0 mm thick crack ($\rho = 1.0$ mm).

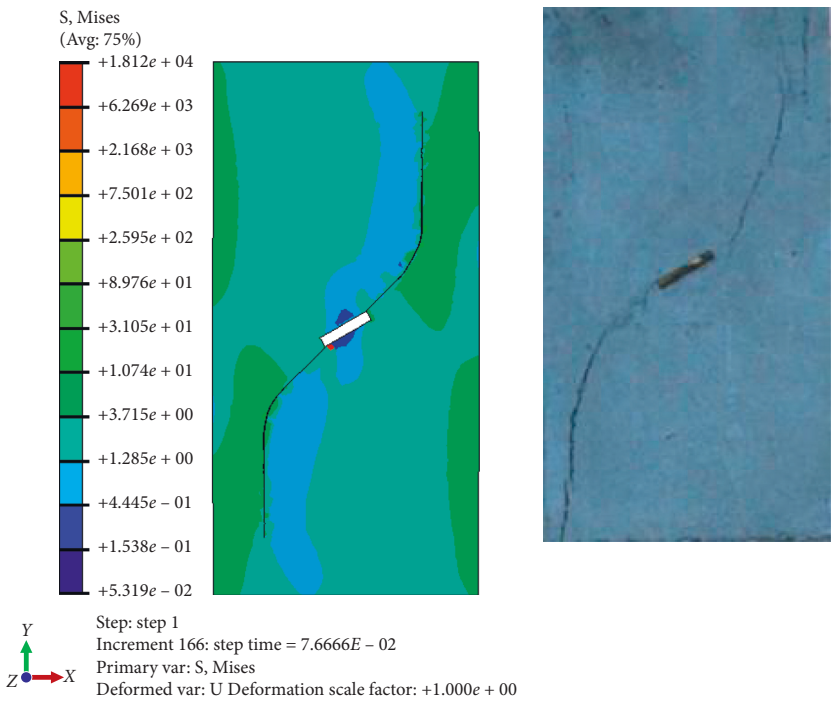

Figure 9: Numerical and experimental results of fracture propagation with 2 mm thick crack and $\beta = 75^{\circ}$: (a) numerical analysis; (b) experimental results.

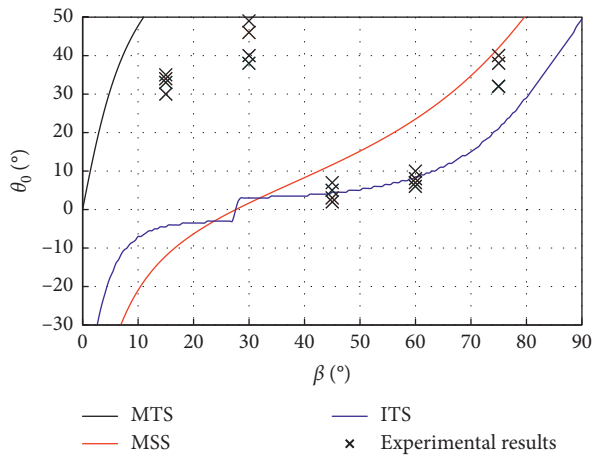

Figure 10: Comparison of initiation angles between theoretical and experimental results.

approximates the direction of the maximum circumferential stress. When the angle between the preloaded crack and the loading direction was large, the crack initiation behavior under loading conformed to the results of the maximum circumferential stress criterion.

(3) MTS faces challenges in interpreting the fracture propagation of open cracks subject to compressional stress. The circumferential compressive stress caused by the mode-I SIF withheld the circumferential tensile stress from the mode-II SIF. For $0 < K_{Ie}/|K_{IIe}| < 1$ and $K_{Ie}/|K_{IIe}| < K_{IC}/K_{IIC}$, the fracture angle of the nonclosed crack was determined by MSS.

Data Availability

The data used to support the findings of this study are included within the article.

Conflicts of Interest

The authors declare that they have no conflicts of interest.

Acknowledgments

The authors thank the project supported by the Funds for Creative Research Groups of China (no. 41521002) and the National Natural Science Foundation of China (no. 41672282). Huang thanks the Innovative Team of the Chengdu University of Technology.

References

[1] A. Bobet and H. H. Einstein, "Fracture coalescence in rock-type materials under uniaxial and biaxial compression," *International Journal of Rock Mechanics and Mining Sciences*, vol. 35, no. 7, pp. 863–888, 1998.

[2] A. Bobet, "The initiation of secondary cracks in compression," *Engineering Fracture Mechanics*, vol. 66, no. 2, pp. 187–219, 2000.

[3] C. H. Park and A. Bobet, "Crack coalescence in specimens with open and closed flaws: a comparison," *International*

Journal of Rock Mechanics and Mining Sciences, vol. 46, no. 5, pp. 819–829, 2009.

[4] M. Sagong and A. Bobet, "Coalescence of multiple flaws in a rock-model material in uniaxial compression," *International Journal of Rock Mechanics and Mining Sciences*, vol. 39, no. 2, pp. 229–241, 2002.

[5] C. A. Tang, P. Lin, R. H. C. Wong, and K. T. Chau, "Analysis of crack coalescence in rock-like materials containing three flaws-Part II: numerical approach," *International Journal of Rock Mechanics and Mining Sciences*, vol. 38, no. 7, pp. 925–939, 2001.

[6] B. Vásárhelyi and A. Bobet, "Modeling of crack initiation, propagation and coalescence in uniaxial compression," *Rock Mechanics and Rock Engineering*, vol. 33, no. 2, pp. 119–139, 2000.

[7] R. H. C. Wong, K. T. Chau, C. A. Tang, and P. Lin, "Analysis of crack coalescence in rock-like materials containing three flaws-Part I: experimental approach," *International Journal of Rock Mechanics and Mining Sciences*, vol. 38, no. 7, pp. 909–924, 2001.

[8] L. Z. Wu, B. Li, R. Q. Huang, and P. Sun, "Experimental study and modeling of shear rheology in sandstone with non-persistent joints," *Engineering Geology*, vol. 222, pp. 201–211, 2017.

[9] L. Z. Wu, H. Deng, R. Q. Huang, L. M. Zhang, X. G. Guo, and Y. Zhou, "Evolution of lakes created by landslide dams and the role of dam erosion: a case study of the Jiajun landslide on the Dadu River, China," *Quaternary International*, vol. 503, pp. 41–50, 2019.

[10] G. R. Irwin, "Analysis of stresses and strains near the end of a crack traversing a plate," *Journal of Applied Mechanics-Transactions*, vol. 22, pp. 361–364, 1957.

[11] A. M. Al-Mukhtar and B. Merkel, "Simulation of the crack propagation in rocks using fracture mechanics approach," *Journal of Failure Analysis and Prevention*, vol. 15, no. 1, pp. 90–100, 2015.

[12] N. A. Al-Shayea, "Crack propagation trajectories for rocks under mixed mode I-II fracture," *Engineering Geology*, vol. 81, no. 1, pp. 84–97, 2005.

[13] Y. P. Li and C. H. Yang, "Influence of geometric characteristics of pre-existing cracks on mixed mode fractures under compression-shear loading," *Chinese Journal of Rock Mechanics and Engineering*, vol. 25, pp. 462–466, 2006.

[14] M. R. Ayatollahi and M. R. M. Aliha, "On the use of Brazilian disc specimen for calculating mixed mode I-II fracture toughness of rock materials," *Engineering Fracture Mechanics*, vol. 75, no. 16, pp. 4631–4641, 2008.

[15] Y. Fujii and Y. Ishijima, "Consideration of fracture growth from an inclined slit and inclined initial fracture at the surface of rock and mortar in compression," *International Journal of Rock Mechanics and Mining Sciences*, vol. 41, no. 6, pp. 1035–1041, 2004.

[16] H. Horii and S. Nemat-Nasser, "Compression-induced microcrack growth in brittle solids: axial splitting and shear failure," *Journal of Geophysical Research*, vol. 90, no. B4, pp. 3105–3125, 1985.

[17] R. P. Janeiro and H. H. Einstein, "Experimental study of the cracking behavior of specimens containing inclusions (under uniaxial compression)," *International Journal of Fracture*, vol. 164, no. 1, pp. 83–102, 2010.

[18] Y.-P. Li, L.-Z. Chen, and Y.-H. Wang, "Experimental research on pre-cracked marble under compression," *International Journal of Solids and Structures*, vol. 42, no. 9-10, pp. 2505–2516, 2005.

[19] H. Lee and S. Jeon, "An experimental and numerical study of fracture coalescence in pre-cracked specimens under uniaxial compression," *International Journal of Solids and Structures*, vol. 48, no. 6, pp. 979–999, 2011.

[20] C. H. Park and A. Bobet, "The initiation of slip on frictional fractures," in *Proceedings of the 41st US Rock Mechanics Symposium*, pp. 06–923, Golden, CO, USA, June 2006.

[21] C. H. Park and A. Bobet, "Crack initiation and propagation from frictional fractures," in *Proceedings of the 1st Canada—US Rock Mechanics Symposium*, pp. 557–564, Vancouver, Canada, May 2007.

[22] C. H. Park and A. Bobet, "Crack initiation, propagation and coalescence from frictional flaws in uniaxial compression," *Engineering Fracture Mechanics*, vol. 77, no. 14, pp. 2727–2748, 2010.

[23] E. Sahouryeh, A. V. Dyskin, and L. N. Germanovich, "Crack growth under biaxial compression," *Engineering Fracture Mechanics*, vol. 69, no. 18, pp. 2187–2198, 2002.

[24] R. H. C. Wong and K. T. Chau, "Crack coalescence in a rock-like material containing two cracks," *International Journal of Rock Mechanics and Mining Sciences*, vol. 35, no. 2, pp. 147–164, 1998.

[25] S.-Q. Yang, "Crack coalescence behavior of brittle sandstone samples containing two coplanar fissures in the process of deformation failure," *Engineering Fracture Mechanics*, vol. 78, no. 17, pp. 3059–3081, 2011.

[26] Y. Zhao, "Crack pattern evolution and a fractal damage constitutive model for rock," *International Journal of Rock Mechanics and Mining Sciences*, vol. 35, no. 3, pp. 349–366, 1998.

[27] L. Z. Wu, G. Q. Shao, R. Q. Huang, and Q. He, "Overhanging rock: theoretical, physical and numerical modeling," *Rock Mechanics and Rock Engineering*, vol. 51, no. 11, pp. 3585–3597, 2018.

[28] C. Tang, "Numerical simulation of progressive rock failure and associated seismicity," *International Journal of Rock Mechanics and Mining Sciences*, vol. 34, no. 2, pp. 249–261, 1997.

[29] A. Manouchehrian, M. Sharifzadeh, M. F. Marji, and J. Gholamnejad, "A bonded particle model for analysis of the flaw orientation effect on crack propagation mechanism in brittle materials under compression," *Archives of Civil and Mechanical Engineering*, vol. 14, no. 1, pp. 40–52, 2014.

[30] H. Dündar and A. O. Ayhan, "Multiple and non-planar crack propagation analyses in thin structures using FCPAS," *Frattura ed Integrità Strutturale*, vol. 10, no. 35, pp. 360–367, 2016.

[31] F. Erdogan and G. C. Sih, "On the crack extension in plates under plane loading and transverse shear," *Journal of Basic Engineering*, vol. 85, no. 4, pp. 519–525, 1963.

[32] M. A. Hussian, E. L. Pu, and J. H. Underwood, "Strain energy release rate for a crack under combined mode I and mode II," in *Proceedings of the Fracture Analysis*, pp. 2–28, ASTM STP 560, West Conshohocken, PA, USA, 1974.

[33] R. J. Nuismer, "An energy release rate criterion for mixed mode fracture," *International Journal of Fracture*, vol. 11, no. 2, pp. 245–250, 1975.

[34] G. C. Sih, "Energy-density concept in fracture mechanics," *Engineering Fracture Mechanics*, vol. 5, no. 4, pp. 1037–1040, 1973.

[35] M. F. Marji, H. Hosseini_Nasab, and A. H. Kohsary, "On the uses of special crack tip elements in numerical rock fracture mechanics," *International Journal of Solids and Structures*, vol. 43, no. 6, pp. 1669–1692, 2006.

[36] M. F. Marji and I. Dehghani, "Kinked crack analysis by a hybridized boundary element/boundary collocation method," *International Journal of Solids and Structures*, vol. 47, no. 7-8, pp. 922–933, 2010.

[37] M. F. Marji, "On the use of power series solution method in the crack analysis of brittle materials by indirect boundary element method," *Engineering Fracture Mechanics*, vol. 98, pp. 365–382, 2013.

[38] B. R. Lawn and T. R. Wilshaw, *Fracture of Brittle Solids*, Cambridge University Press, London, UK, 1975.

[39] N. I. Muskhelishvili, *Some Basic Problems of the Mathematical Theory of Elasticity*, Noordhoff International Publishing, Leyden, The Netherlands, 1953.

[40] G. C. Sih, *Mechanics of Fracture*, Noordhoff International Publishing, Leyden, The Netherlands, 1973.

[41] L. Z. Wu, B. Li, R. Q. Huang, and Q. Z. Wang, "Study on Mode I-II hybrid fracture criteria for the stability analysis of sliding overhanging rock," *Engineering Geology*, vol. 209, pp. 187–195, 2016.

[42] M.-H. Yu, "Twin shear stress yield criterion," *International Journal of Mechanical Sciences*, vol. 25, no. 1, pp. 71–74, 1983.

[43] T. Backers and O. Stephansson, "ISRM suggested method for the determination of mode II fracture toughness," *Rock Mechanics and Rock Engineering*, vol. 45, no. 6, pp. 1011–1022, 2012.

[44] ABAQUS Inc, *ABUQUS/Standard User's Manual Version 6.9*, ABAQUS Inc, Waltham, MA, USA, 2009.

[45] R. Q. Huang, L. Z. Wu, Q. He, and J. H. Li, "Stress intensity factor analysis and the stability of overhanging rock," *Rock Mechanics and Rock Engineering*, vol. 50, no. 8, pp. 2135–2142, 2017.

[46] M. L. Benzeggagh and M. Kenane, "Measurement of mixed-mode delamination fracture toughness of unidirectional glass/epoxy composites with mixed-mode bending apparatus," *Composites Science and Technology*, vol. 56, no. 4, pp. 439–449, 1996.